ELSEVIER

NeuroImage

www.elsevier.com/locate/ynimg
NeuroImage 24 (2005) 874–886

Identification of the neural sources of the pattern-reversal VEP

Francesco Di Russo,[a,b,*] Sabrina Pitzalis,[b,c] Grazia Spitoni,[b,c] Teresa Aprile,[b,c] Fabiana Patria,[b] Donatella Spinelli,[a,b] and Steven A. Hillyard[d]

[a]*Istituto Universitario di Scienze Motorie (IUSM), Rome, Italy*
[b]*Fondazione Santa Lucia, IRCCS, Rome, Italy*
[c]*Department of Psychology, University of Rome "La Sapienza," Rome, Italy*
[d]*Department of Neurosciences, UCSD, La Jolla, CA 92037, USA*

Received 29 June 2004; revised 15 September 2004; accepted 21 September 2004
Available online 13 November 2004

This study aimed to characterize the neural generators of the early components of the visual-evoked potential (VEP) to pattern-reversal gratings. Multichannel scalp recordings of VEPs and dipole modeling techniques were combined with functional magnetic resonance imaging (fMRI) and retinotopic mapping in order to estimate the locations of the cortical sources giving rise to VEP components in the first 200 ms poststimulus. Dipole locations were seeded to visual cortical areas in which fMRI activations were elicited by the same stimuli. The results provide strong evidence that the first major component of the VEP elicited by a pattern-reversal stimulus (N75/P85) arises from surface-negative activity in the primary visual cortex (area V1). Subsequent waveform components could be accounted for by dipoles that were in close proximity to fMRI activations in the following cortical areas: P95 (area MT/V5), P125/N135 (area V1), N150 (transverse parietal sulcus, TPS), N160 (ventral occipital areas VP, V4v, and V4/V8), and N180 (dorsal occipital areas V3A/V7). These results provide a detailed spatiotemporal profile of the cortical origins of the pattern-reversal VEP, which should enhance its utility in both clinical and basic studies of visual-perceptual processing.

Keywords: Pattern reversal; Visual-evoked potential; Dipoles; MRI; fMRI; Retinotopic mapping; V1; ERP; Co-registration; Visual quadrants

Introduction

Studies of transient visual-evoked potentials (VEPs) in humans have used stimulus patterns presented briefly in on–off mode (pattern onset) as well as counterphase shifts of gratings or checkerboards (pattern reversal). Pattern-onset VEPs are characterized by an initial component at 70–90 ms after stimulus onset (the C1 component) that varies in polarity according to stimulus position, followed by a positive wave at 100–130 ms (P1 component) and a negative wave complex at 140–190 ms (N1 component). Conflicting proposals have been advanced regarding the neural generators of these components in striate and extrastriate cortical areas (reviewed in Clark et al., 1995). Recent studies that combined dipole modeling with functional magnetic resonance imaging (fMRI) of activated cortical areas have provided evidence that the C1 component to pattern onset is generated in the primary visual cortex (area V1) while the early part of the P1 wave arises from generators in the dorsal extrastriate occipital cortex and the later part of the P1 from sources in ventral extrastriate cortex (Di Russo et al., 2001, 2003; Martinez et al., 1999, 2001). These studies localized the generators of the early, anterior part of the N1 complex to posterior parietal cortex and the later posteriorly distributed N1 to the same occipital generators as the P1.

The VEP elicited by a reversing pattern (e.g., checkerboard) is characterized by an initial negative component peaking at around 75 ms after the reversal (N75) followed by a positive component at around 100 ms (P100) and a second negativity at around 145 ms (N145) (Halliday, 1993). As with the pattern-onset VEP, the neural generators of the pattern-reversal VEP components have been much debated. While there is widespread agreement (based on studies in both animals and humans) that the N75 of the pattern-reversal VEP originates from the primary visual cortex (see Table 1), the origin of the P100 component is controversial. Some investigators have suggested that the P100 (like the pattern-onset P1) is mainly generated in extrastriate visual areas, while the majority has proposed that the P100 is generated (like the N75) in the striate cortex. N145 has been studied less extensively than the two earlier components. Some studies have identified a source for N145 in the extrastriate visual cortex, while others concluded that the N145 arises from the calcarine cortex or from both striate and extrastriate areas.

* Corresponding author. Dip. di Scienze della Formazione per le Attività Motorie e lo Sport, Istituto Universitario di Scienze Motorie, IUSM, Piazza L. De Bosis, 15 (Foro Italico). 00194 Rome, Italy.
E-mail address: fdirusso@iusm.it (F. Di Russo).
URL: http://bioingegneria.iusm.it/psicologia/fdr.
Available online on ScienceDirect (www.sciencedirect.com).

1053-8119/$ - see front matter © 2004 Elsevier Inc. All rights reserved.
doi:10.1016/j.neuroimage.2004.09.029

Table 1
Conclusions of previous studies regarding the visual–cortical areas that generate the first (N75), second (P100), and third (N145) major components of the pattern-reversal VEP

Authors	Technique	N75	P100	N145
Michael and Halliday, 1971	VEP	V1		
Barrett et al., 1976	VEP		V1	
Lehmann et al., 1982	VEP		V2–V3	
Haimovic and Pedley, 1982	VEP		V1	
Hoeppner et al., 1984	VEP		V1	
Maier et al., 1987	VEP	V1		
Biersdorf, 1987	VEP	V1	V1	
Ducati et al., 1988	VEP	V1	V1	
Onofrj et al., 1993	VEP	V1	V2/V3	
Noachtar et al., 1993	VEP	V1	V1–V2	V2–V3
Schroeder et al., 1995	VEP	V1–V2	V3–V4	V2–V3
Onofrj et al., 1995a	VEP	V1	V2/V3	
Onofrj et al., 1995b	VEP	V2	V2/V3	V2/V3
Nakamura et al., 1997	VEP/MEG		VI	
Seki et al., 1996	MEG		V1	
Hatanaka et al., 1997	MEG	V1	V1	V1
Brecelj et al., 1998	VEP/MEG		V1	
Shigeto et al., 1998	VEP/MEG	V1	V1	V1
Slotnick et al., 1999	VEP		V1	
Hashimoto et al., 1999	VEP/MEG	V1	V1	V1
Nakamura et al., 2000	VEP/MEG		VI	
Vanni et al., 2001	MEG	V1	Extrastriate	
Bonmassar et al., 2001	VEP/fMRI	V1	V1	
Tobimatsu, 2002	VEP/MEG	V1	V1	V1
Tabuchi et al., 2002	MEG	V1	V1	

Despite uncertainties as to the neural origins of its components, the pattern-shift VEP has had wide applications in clinical studies of visual system dysfunction (Halliday, 1993).

This lack of agreement among previous studies may be due to methodological differences such as the number of recording sites and the type of stimuli used. In particular, a sparse electrode array may not be able to differentiate concurrent activity arising from neighboring visual areas nor to obtain an accurate picture of the voltage topography produced by a given source. Furthermore, the use of stimuli extending over wide visual angles in some studies might have activated widespread regions of retinotopic cortical areas, thereby reducing the possibility of identifying the exact generator locations. In particular, stimuli that span more than one visual quadrant (crossing the horizontal and vertical meridians) may lead to activation of neuronal populations with opposing geometry (as in the primary visual area) resulting in a cancellation of their electric activity and in misinterpretation of the underlying source.

The purpose of the present study was to determine the detailed component structure of the pattern-reversal VEP and to localize its neural generators by using focal stimulation of each of the visual quadrants and a dense recording array of 64 electrodes. Sources were identified using dipole modeling based on a realistic head model and were compared with loci of cortical activations revealed by fMRI in response to the same stimuli. These sources were also localized on flat map with respect to visual cortical areas identified in individual subjects by retinotopic mapping and motion stimulation.

Materials and methods

Subjects

Twenty-five paid volunteer subjects (12 female, mean age 26.1, range 18–36 years) participated in the VEP recordings. A subset of six of these subjects (three female, mean age 26.8, range 23–35 years) also received anatomical MRI scans and participated in the fMRI study. All subjects were right-handed and had normal or corrected-to-normal visual acuity. Written informed consent was obtained from all subjects after the procedures had been fully explained to them.

Stimuli

The stimuli consisted of brief phase shifts of circular Gabor gratings that were sinusoidally modulated in black and white and horizontally oriented (Fig. 1); stimulus diameter was 2° of visual angle with a spatial modulation frequency of 4 cycles/degree. Each stimulus consisted of a 180° phase shift of the grating lasting 66 ms with an immediate return to the original phase. The background luminance (22 cd/m^2) was isoluminant with the mean luminance of the grating pattern, which was modulated at a contrast of 32%. In the VEP experiment, phase-shift stimuli were presented one at a time in randomized order to the four quadrants of the visual fields at a fast rate (SOAs varying between 350 and 650 ms). Stimulus positions were centered along an arc that was equidistant (4°) from a central fixation point and located at polar angles of 25° above and 45° below the horizontal meridian. These asymmetrical positions were chosen so that the upper and lower field stimuli would stimulate approximately opposite zones of the lower and upper banks of the calcarine fissure, respectively, based on findings that the horizontal meridian is actually represented on the lower bank rather than at the lateral recess of the calcarine fissure (Aine et al., 1996; Clark et al., 1995; Di Russo et al., 2001, 2003).

In the fMRI experiment, the same stimuli were presented at the same locations and rate but only in one quadrant at a time instead of in random order.

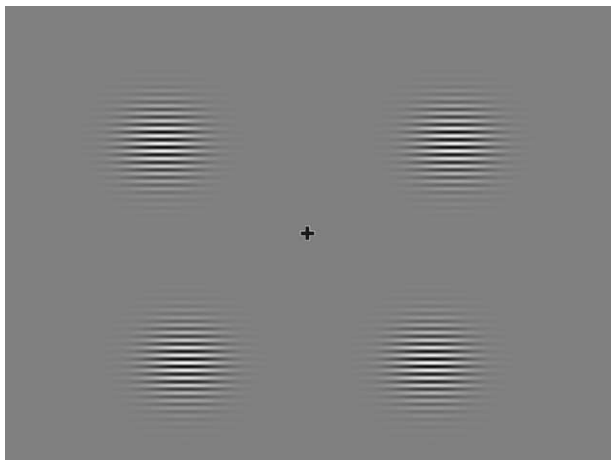

Fig. 1. Stimuli used in this experiment. Circular Gabor gratings were phase reversed at one of the four locations at a time in random order.

Procedure

In the VEP experiment, the subject was comfortably seated in a dimly lit sound-attenuated and electrically shielded room while stimuli were presented in binocular vision on a video monitor at a viewing distance of 114 cm. Subjects were trained to maintain stable fixation on a central cross (0.2°) throughout stimulus presentation. Each run lasted 120 s followed by a 30-s rest period, with longer breaks interspersed. A total of 18 runs were carried out in order to deliver at least 800 phase-shift stimuli to each quadrant. The subjects were given feedback on their ability to maintain fixation.

For the fMRI experiment, one visual quadrant was stimulated in each run, alternating 16 s of stimulation (pattern reversals) with 16 s of no stimulation (pattern present but steady) for 8 cycles. This sequence was repeated at least three times for each quadrant.

Electrophysiological recording and data analysis

The EEG was recorded from 64 electrodes placed according to the 10–10 system montage (see Di Russo et al., 2001). All scalp channels were referenced to the left mastoid (M1). Horizontal eye movements were monitored with a bipolar recording from electrodes at the left and right outer canthi. Blinks and vertical eye movements were recorded with an electrode below the left eye, which was referenced to site Fp1. The EEG from each electrode site was digitized at 250 Hz with an amplifier bandpass of 0.01–60 Hz including a 50-Hz notch filter and was stored for off-line averaging. Computerized artifact rejection was performed prior to signal averaging in order to discard epochs in which deviations in eye position, blinks, or amplifier blocking occurred. On average, about 11% of the trials were rejected for violating these artifact criteria. VEPs were averaged separately for stimuli in each quadrant in epochs that began 100 ms prior to the phase shift and lasted for 1100 ms. To further reduce high-frequency noise, the averaged VEPs were low-pass filtered at 35 Hz. The amplitudes of the different VEP components were measured as peak values within specified windows with respect to the 100 ms prestimulus baseline.

fMRI scanning and analysis

Subjects were selected for participation in fMRI scanning on the basis of their ability to maintain steady visual fixation as assessed by electrooculographic recordings during the VEP recording sessions. Imaging was carried out with a Siemens VISION scanner (1.5 T) retrofitted for echo-planar imaging. Single-shot EPI images were collected using a custom-built Small Flex quadrature surface RF coil placed over occipital and parietal areas.

Stimuli were presented on a back-projection screen and viewed with a mirror at an average distance of 21 cm. Head motion was minimized by using a bite bar having an individually molded dental impression mounted on a locking Plexiglas arm together with foam pads around the subject's head. Interior surfaces were covered with black velvet to eliminate reflections. Subjects were required to maintain fixation on a central point during all scans.

Single subject data analysis

The boundaries of the retinotopic visual areas were defined in each participant using the field-sign method. The 'field sign' for each cortical area was calculated from the constituent phase-encoded maps of polar angle (angle from the center-of-gaze) and eccentricity (distance from the center-of-gaze) using standard stimuli for retinotopic mapping (Sereno et al., 1995; Tootell et al., 1997). The phase-encoded stimuli spared a central 0.75° circular zone of the visual field to avoid ambiguities caused by fixation instability. Additional scans were acquired to localize the motion-sensitive area MT/V5 (MT mapping); in a block design sequence, moving and stationary patterns of low contrast (multiple rings surrounding the central fixation point) were alternated in 32-s epochs for 8 cycles/scan, as described elsewhere (Dumoulin et al., 2003; Tootell and Taylor, 1995).

Scans for retinotopic mapping lasted 8 min 32 s (TR = 4 s), and scans for pattern-reversal stimulation of each quadrant lasted 4 min 16 s (TR = 2 s). In each scan, the first 8 s of the acquisition was discarded from data analysis in order to achieve a steady state. Each scan included 2048 images, comprised of 128 images per slice in 16 or 24 contiguous slices (TE = 42, flip angle = 90°, 64 × 64 matrix, bandwidth = 926 Hz/pixel, 8 stimulus cycles. MR slices were 4 mm thick, with an in-plane resolution of 3 × 3 mm, oriented approximately perpendicular to the calcarine fissure. A total of 90 functional scans were carried out on the six subjects (24 scans to map the retinotopic visual areas, 18 scans to map MT/V5, and 48 scans for the pattern-reversal quadrant stimulation). The cortical surface for each subject was reconstructed from a pair of structural scans (T1-weighted MPRAGE, TR = 11.4 ms, TE = 4.4 ms, flip angle = 10°, 1 × 1 × 1 mm resolution) taken in a separate session using a head coil. The last scan of each functional session was an alignment scan (also MPRAGE, 1 × 1 × 1 mm) acquired with the surface coil in the plane of the functional scans. The alignment scan was used to establish an initial registration of the functional data with the surface. Additional affine transformations that included a small amount of shear were then applied to the functional scans for each subject using blink comparison with the structural images to achieve an exact overlay of the functional data onto each cortical surface. To improve the signal to noise ratio, we typically averaged data together from three scans for each stimulus type (pattern-reversal quadrant stimulation, retinotopy, and MT/V5 mapping). Processing of functional and anatomical images was performed using FreeSurfer (Dale et al., 1999; Fischl et al., 1999. Available on-line at http://surfer.nmr.mgh.harvard.edu/.

All data were initially analyzed by making a fast Fourier transform of the MR time course from each voxel. Statistical significance was calculated and displayed by converting the Fourier magnitude of the response to an F statistic. The phase of the response at the stimulus frequency was used to track stimulus location in the case of retinotopic stimuli and to distinguish between positive- and negative-going MR fluctuations in the case of stimulus vs. no-stimulus comparisons. All effects were analyzed and displayed in cortical surface format, as described elsewhere (Felleman and Van Essen, 1991; Schiller and Dolan, 1994). This made it possible to extract the MR time courses from voxels in specific cortical areas, which were defined in the same subjects. The specific areas sampled were V1, V2, V3/VP, V3A, V4v, V7, and MT/V5. Above a minimum threshold, the statistical significance of the displayed pseudocolor range has been normalized according to the overall sensitivity of each subject, as described elsewhere (Hadjikhani et al., 1998).

Group data analysis

Group data analysis was performed with SPM99 (Wellcome Department of Cognitive Neurology). Functional images from each participant were co-aligned with the high-resolution anatomical

scan (MPRAGE) taken in the same session. Images were motion corrected through a rigid body transformation with a least squares approach and transformed into normalized stereotaxic space (Talairach and Tournoux, 1988). A fixed-effects general linear model was employed to compute statistical maps for the group average. The experimental conditions were modeled as simple box-car functions (stimulus vs. no-stimulus condition) and convolved with a synthetic hemodynamic response function. Statistical significance of activated regions was assessed by using a probability criterion of $P \leq 0.01$ corrected at the voxel level. The statistical parametric maps were superimposed onto the standard brain supplied by SPM99 and flattened with the FreeSurfer software.

Modeling of VEP sources

Topographical maps of scalp voltage over time were obtained for the VEPs to stimuli in each of the four quadrants. Estimation of the dipolar sources of VEP components was carried out using Brain Electrical Source Analysis (BESA 2000 version 5). The BESA algorithm estimates the location and the orientation of multiple equivalent dipolar sources by calculating the scalp distribution that would be obtained for a given dipole model (forward solution) and comparing it to the actual VEP distribution. Interactive changes in the location and orientation in the dipole sources lead to minimization of the residual variance (RV) between the model and the observed spatiotemporal VEP distribution. This analysis used a realistic approximation of the head with the radius obtained from the average of the group of subjects (91 mm). A spatial digitizer recorded the three-dimensional coordinates of each electrode and of three fiducial landmarks (the left and right preauricular points and the nasion). A computer algorithm was used to calculate the best-fit sphere that encompassed the array of electrode sites and to determine their spherical coordinates. The mean spherical coordinates for each site averaged across all subjects were used for the topographic mapping and source localization procedures. In addition, individual spherical coordinates were related to the corresponding digitized fiducial landmarks and to landmarks identified on the standardized finite element model of BESA 2000.

A proximity seeding strategy was used to model the dipolar sources of the VEP. First, an unseeded model was fit over specific latency ranges (given below) to account for the major VEP waveform features. Next, loci of fMRI activation in close proximity to those dipoles were identified and were used to constrain the locations of the dipoles in a new seeded model. In the unseeded model, single dipoles or pairs were fit sequentially to the distinctive components in the waveform. The latency ranges for fitting were chosen to minimize overlap among the successive, topographically distinctive components. Dipoles accounting for the earlier portions of the waveform were left in place as additional dipoles were added. The reported dipole fits were found to remain consistent for different starting positions. For dipole pairs, the dipole ipsilateral to the stimulated visual field was constrained to be a mirror image of the contralateral dipole in location only.

The dipole fitting strategy was as follows: a single dipole was fit to the N75/P85 component based on its midline scalp topography. The subsequent P95, N150, and N160 components were fit with bilateral mirror symmetric pairs of dipoles on the basis of both present and previous topographical mapping evidence showing that components in this latency range have mirror image foci over the contralateral and ipsilateral occipital scalp, with the ipsilateral focus delayed by about 10–30 ms (i.e., Di Russo et al., 2001, 2003). Visual mapping studies with fMRI (e.g., Tootell et al., 1998) have also shown that visual areas tend to show a substantial degree of bilateral symmetry. Most early visual areas beyond V1 have callosal connections that produce some degree of bilateral activation to unilateral stimulation. The present fMRI data also indicated the presence of bilateral, mirror-symmetric activations in extrastriate cortical areas. In the seeded model, dipoles were constrained in location to the centers of the group-averaged fMRI activations nearest to the unseeded dipoles, and their orientations were re-fit over the same time intervals used in the unseeded model.

Results

VEP waveforms and topography

The VEP waveforms elicited at selected electrode sites by stimuli in each of the four quadrants are shown in Fig. 2. The amplitudes, latencies, and topographical features of the major components are listed in Table 2.

The earliest component (here termed N75/P85) had a peak latency of 75–85 ms and inverted in polarity for upper vs. lower field stimuli. For upper field stimuli, the N75 was most prominent at occipitoparietal sites slightly ipsilateral to the midline (see Fig. 3 for scalp distributions). For lower field stimuli, this component (P85) reversed in polarity and was largest at occipitoparietal sites slightly contralateral to the midline. The difference in peak latency between the upper field N75 and the lower field P85 was not significant ($t_{(24)} = 1.29$).

Overlapping in time with the N75/P85 component was a positive deflection (P95) elicited over contralateral occipitotemporal sites with a peak latency of 92 ms for the upper field and 96 ms for the lower field stimuli. This latency difference was not significant and was most likely attributable to overlap with the polarity inverting N75/P85. P95 did not change in polarity for stimuli in the upper vs. lower hemifields. A subsequent positivity (P125) was evoked by upper field stimuli with a midline occipitoparietal distribution very similar to that of the N75. A corresponding negative component (N135) was elicited by lower field stimuli with a distribution very similar to that of the P85. The P125/N135 components thus had distributional and polarity-inverting characteristics closely resembling those of the earlier N75/P85. The small latency difference between the P125 and the N135 did not reach significance.

In the interval between 140 and 180 ms, several spatially and temporally overlapping negative waves were elicited concurrently. An initial negative peak (N150) was prominent at contralateral midline central sites for all quadrants. A second negative deflection (N160) had a contralateral occipitoparietal distribution for lower field stimuli and a more bilateral distribution for upper field stimuli. A third negative component (N180) was distributed over contralateral temporoparietal sites. These components did not change appreciably in latency for stimuli in the upper vs. lower visual fields.

fMRI activations

Sensory-evoked fMRI activations were observed in multiple visual cortical areas including the calcarine cortex, the posterior

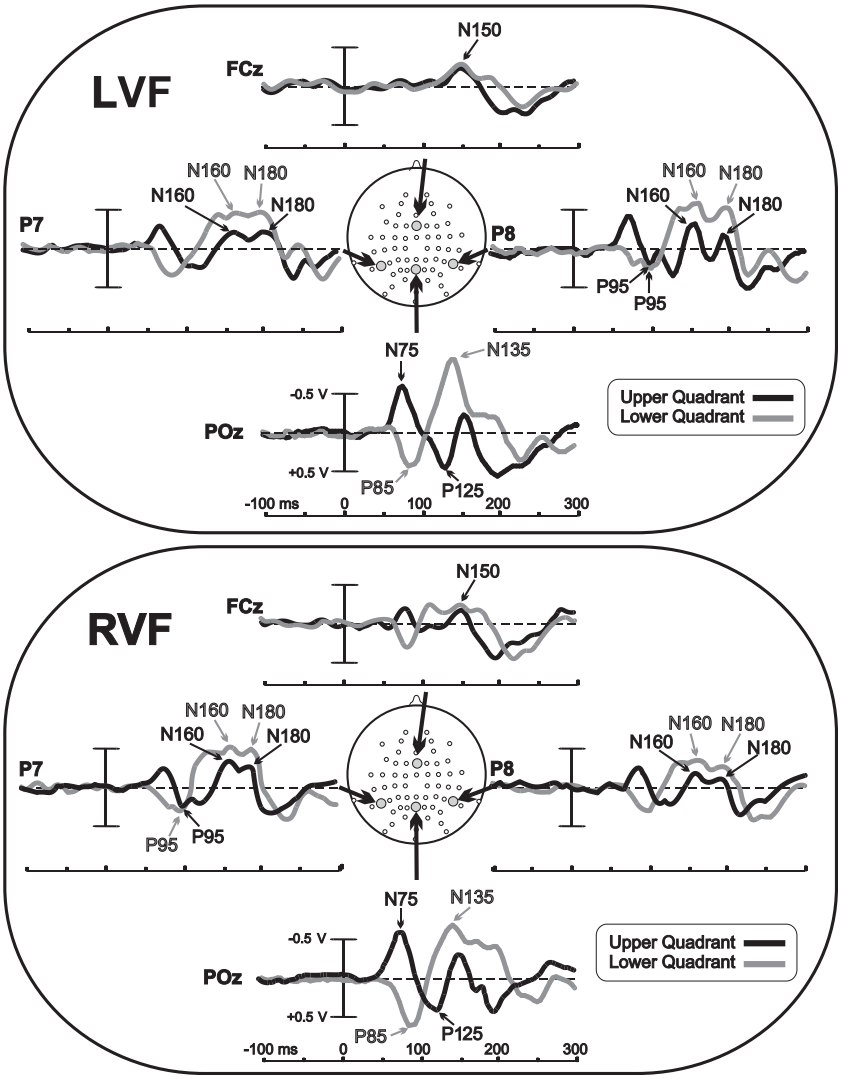

Fig. 2. Grand averaged VEPs to stimuli located in the upper (black tracings) and lower (gray tracings) quadrants of the left (upper panel) and right (lower panel) visual fields. Recordings are from midline fronto-central (FCz) and left (P7), right (P8), and midline (POz) parietooccipital sites.

end of the intraparietal sulcus (pIPS) and its neighboring sulci, the fusiform gyrus, the middle temporal sulcus (MTS), and the transverse parietal sulcus (TPS). In the extrastriate areas, the contralateral and ipsilateral activations were approximately mirror-image symmetric (Table 3). Fig. 4 shows the group-averaged contralateral fMRI activations to stimuli in each

Table 2
Topography, amplitudes (μV), and latencies (ms) of different VEP components

Component	Stimulus position	Topography	Measurement electrode	Peak amplitude	Peak latency
N75	Upper	Ipsilateral	PO1/PO2	−0.55	76
P85	Lower	Contralateral	PO3/PO4	0.54	84
P95	Upper	Contralateral	I5/I6	0.18	92
	Lower	Contralateral	I3/I4	0.20	94
P125	Upper	Ipsilateral	PO1/PO2	0.41	126
N135	Lower	Contralateral	PO3/PO4	−0.66	134
N150	Upper	Contralateral	FC1/FC2	−0.25	146
	Lower	Contralateral	FC1/FC2	−0.22	148
N160	Upper	Bilateral	P5/P6	−0.34	160
	Lower	Contralateral	PO3/PO4	−0.72	164
N180	Upper	Contralateral	P7/P8	−0.16	182
	Lower	Contralateral	PO7/PO8	−0.53	184

Latency and amplitude measures were averaged over VEPs to stimuli in left and right visual fields.

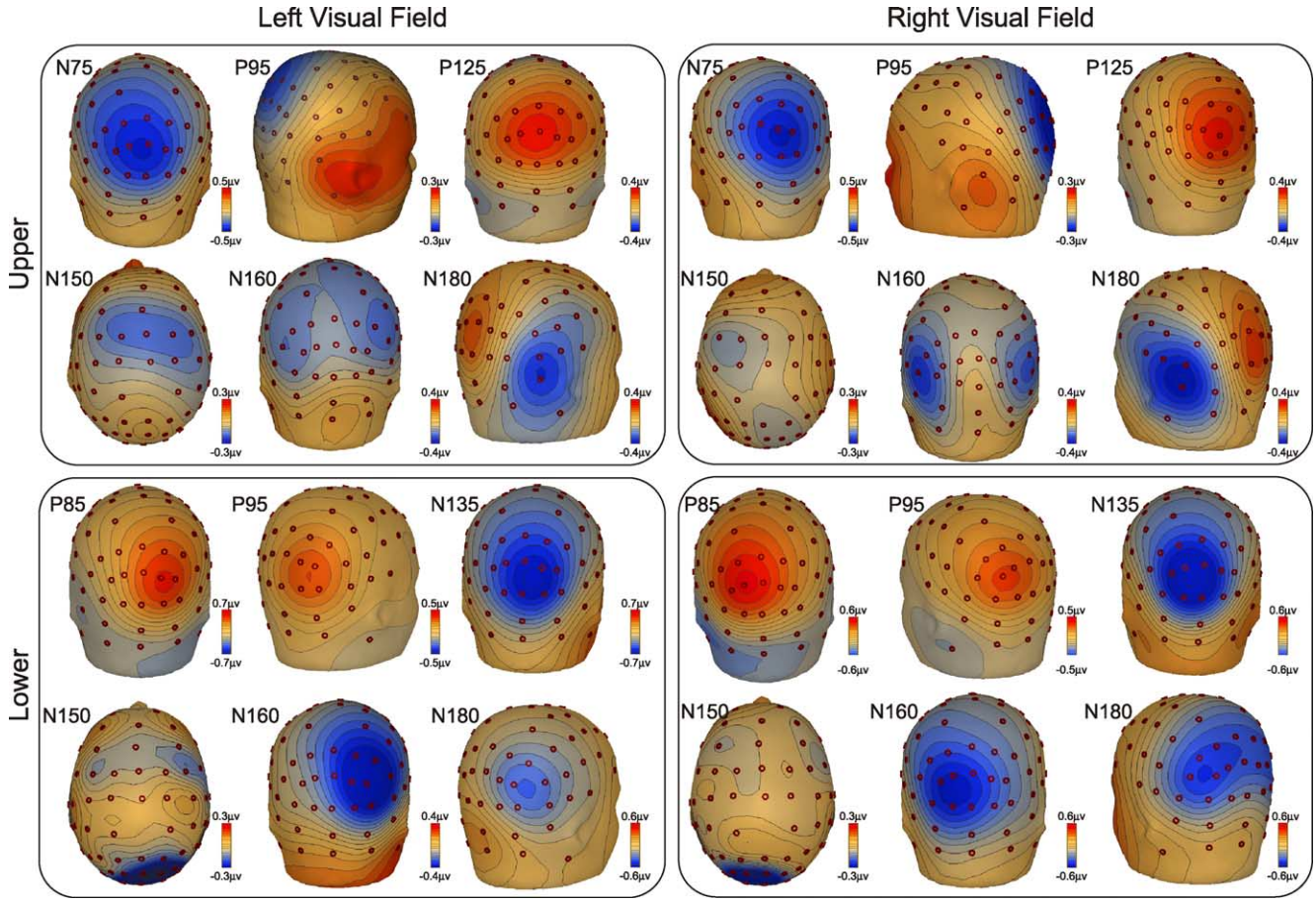

Fig. 3. Spline-interpolated three-dimensional voltage maps of VEP components elicited by stimuli in each quadrant. Latencies of maps are at peaks indicated in Table 2.

quadrant superimposed on the flattened cortical surface of the MNI template.

Stimulus-evoked fMRI activations were localized with respect to the retinotopically organized visual areas defined on the basis of their calculated field signs (Sereno et al., 1995), and to area MT/V5 as defined by motion mapping. The borders of retinotopically organized visual areas (V1, V2, V3, VP, V3A, V4v, and V7) and area MT/V5 could be identified for each subject, and activations in striate and adjacent extrastriate visual areas could be distinguished despite their close proximity and individual differences in cortical anatomy. As shown in Fig. 5, upper quadrant stimuli produced activations in the lower banks of areas V1 and V2 as well as in areas VP, V3A+, V4v, and MT/V5. Lower quadrant stimuli produced activations in the upper banks of V1 and V2, and in areas V3, V3A−, and MT/V5; additional activations were found in a region located in the fusiform gyrus just anterior to V4v. This area (not labeled in Fig. 5) most likely corresponds to the color-sensitive area that has been called V4 (Lueck et al., 1989; Zeki and Bartels, 1999) or V8 (Hadjikhani et al., 1998; Tootell and Hadjikhani, 2001). This fusiform region also responds to upper quadrant stimulation, as shown in the group data of Fig. 4 and as reported in previous fMRI studies (e.g., Di Russo et al., 2001; Hadjikhani et al., 1998). For both upper and lower field stimuli, there were loci of activation in the parietal cortex, specifically in the transverse parietal sulcus (TPS) located medially with respect to the intraparietal sulcus (IPS).

Dipole modeling

Inverse dipole modeling of the early VEP components in the time range 60–190 ms was carried out on the grand average waveforms using the BESA 2000 algorithm. Separate dipole models were calculated for each of the four quadrants (Fig. 6a). The first step of the modeling strategy was to fit an unseeded model to the major waveform features as follows: (1) a single dipole was fit over the 60- to 80-ms interval, which accounted for the N75/P85 component for each quadrant. These single dipoles were localized to medial posterior occipital cortex, and their source waveforms also provided a good account of the subsequent P125/N135 components. (2) A dipole pair fit over the 80- to 120-ms time window accounted well for the P95 component and was localized in dorsomedial occipital cortex; the source waveforms of this dipole pair showed a second peak of activity at around 185 ms. (3) A second dipole pair fit over 135–155 ms accounted for the N150 component and was localized in the parietal cortex. (4) A third dipole pair fit over 150–170 ms accounted for the N160 component and was located in the ventral occipital cortex. In all quadrants, these multidipole models accounted for more than 96% of the variance in scalp voltage topography over the time range 60–190 ms (Fig. 6a and Table 4).

Comparing the unseeded dipole coordinates with those of the fMRI activations in response to the same stimuli (compare Tables 3 and 4), it appears that the two techniques yielded partially convergent results. The single dipoles accounting for the N75/

Table 3
Talairach coordinates of the significant striate, extrastriate, and parietal activation sites in the average fMRI data over six subjects

Upper left	LH ipsilateral			RH contralateral			Upper right	LH contralateral			RH ipsilateral		
	x	*y*	*z*	*x*	*y*	*z*		*x*	*y*	*z*	*x*	*y*	*z*
Calcarine	–	–	–	7	−90	2	Calcarine	−6	−87	2	–	–	–
pIPS	−36	−76	19	31	−80	13	pIPS	−26	−85	18	29	−81	22
Fusiform	−27	−74	−7	30	−70	−10	Fusiform	−28	−70	−8	33	−74	−10
MTS	−44	−69	1	42	−71	0	MTS	−43	−69	3	40	−71	−1
TPS	−24	−76	32	26	−75	37	TPS	−25	−74	33	30	−76	28
Lower left	*x*	*y*	*z*	*x*	*y*	*z*	Lower right	*x*	*y*	*z*	*x*	*y*	*z*
Calcarine	–	–	–	10	−85	15	Calcarine	−9	−84	12	–	–	–
pIPS	−31	−76	18	35	−78	22	pIPS	−21	−79	27	25	−76	23
Fusiform	−33	−61	−14	34	−60	−12	Fusiform	−32	−72	−10	30	−74	−8
MTS	−46	−75	1	43	−73	2	MTS	−45	−69	5	41	−64	3
TPS	−26	−72	39	24	−74	35	TPS	−30	−61	47	26	−67	41

Coordinates of activations in right (RH) and left (LH) hemispheres are given for stimuli in each of the four quadrants (values are in mm).

P85 were in close proximity to the V1 activations obtained in the fMRI experiment. A consistent correspondence was also found between the locations of the parietal N150 dipoles and the fMRI activations in and around the transverse parietal sulcus (TPS) and between the ventral N160 dipoles and the V4v/VP activations. The dorsal dipole fit to the P95, however, was about equidistant from the V5 and V3A activations.

For the seeded model (Fig. 6b), the dipole positions were shifted to correspond to the locations of the neighboring fMRI foci of activation (Table 3) and were fit only in orientation within the same time windows as for the unseeded model. The order of dipole fitting was as follows: (1) a single dipole was placed on the V1 activation and fit over 60–80 ms to account for the N75/P85 component; (2) the contralateral dipole of a symmetrical pair was placed at the parietal fMRI location and fit over 135–155 ms to account the N150 component; (3) the contralateral dipole of a second symmetrical pair was placed at the VP/V4v locus of activity and optimized in the 150–170 ms windows to account for the N160 component; (4) because the unseeded dipole fit to the P95 was about equidistant from the MT/V5 and V3A activations and its source waveform showed two temporally distinct peaks (95 and 185 ms), this waveform was modeled by two pairs of dipoles that were placed at the MT/V5 and V3A activations, respectively. The dipole pair at MT/V5 was fit over 80–120 ms to account for the P95 and the pair at V3A was fit over 160–190 ms to account for the later peak; fitting these dipoles in the reverse order yielded a less accurate model.

From the source waveforms of the seeded model (Fig. 6b), it can be seen that the dipoles placed at V1 accounted for both the N75/P125 (upper field) and the P85/N135 (lower field) components. These dipoles showed a polarity inversion between upper vs. lower field stimuli that was approximately 180° in the sagittal plane. The dipole pair seeded to area MT/V5 provided a good fit to the P95 component, and its source waveforms indicated that it also accounted for a subsequent negativity at 130–140 ms. The seeded parietal dipole pair showed a peak of activity at 145–155 ms and accounted well for the anterior N150 topography. The dipoles seeded to the ventral occipital activations (VP/V4v upper field, V4/V8 upper and lower fields) had source waveforms peaking at 160–165 ms that corresponded to the N160 component. Finally, the dipoles seeded to the V3A location had source waveforms with positive activity in the 130–140 ms range as well as a later negativity at 180–190 ms that corresponded to the N180. For all dipole pairs, the components in the ipsilateral source waveforms lagged those in the contralateral waveforms by 10–20 ms. These multidipole models each accounted for more than 98% of the variance in scalp voltage topography for each quadrant over the time range 60–190 ms.

Discussion

The present results provide strong support for the hypothesis that the first major component of the VEP elicited by a pattern reversal stimulus (N75/P85) arises from surface-negative activity in the primary visual cortex (area V1). The scalp topography of this component, its short onset latency, retinotopic polarity inversion, and dipole source localization in conjunction with structural and functional MRI all point to a neural generator in area V1 within the calcarine fissure. This conclusion is in accordance with the findings of a number of previous studies (see Introduction and Table 1), but the present experiment is the first to our knowledge to provide converging evidence from fMRI with retinotopic mapping in support of a striate cortex generator.

The N75/P85 observed here to pattern-reversal stimuli has strong similarities to the C1 elicited by pattern-onset stimuli (Clark et al., 1995; Di Russo et al., 2001). Both components show maximal amplitudes at midline parietooccipital sites and an inversion in polarity in response to changes in stimulus position between upper and lower quadrants in accordance with the cruciform model of primary visual cortex. This inversion was verified by dipole modeling that showed a near 180° rotation of the corresponding dipole for upper vs. lower field stimuli. Further evidence supporting a striate generator for both the N75/P85 and C1 components came from high-resolution structural MRI images with superimposed fMRI activations and retinotopic mapping. Dipoles seeded to the sites of fMRI activation in V1 provided an excellent account of the topography and time course of both the N75/P85 and C1 (Di Russo et al., 2001) components. These similarities suggest that the C1 to pattern onset and the P75/85 to pattern-reversal stimuli arise from common patterns of synaptic activation producing a surface-negative field in striate cortex.

In the case of pattern-reversal stimulation, N75/P85 was followed by a second polarity-inverting component (P125/N135) that was localized to the same dipolar source in V1. In the pattern-onset condition, C1 was not followed by such a component. It is

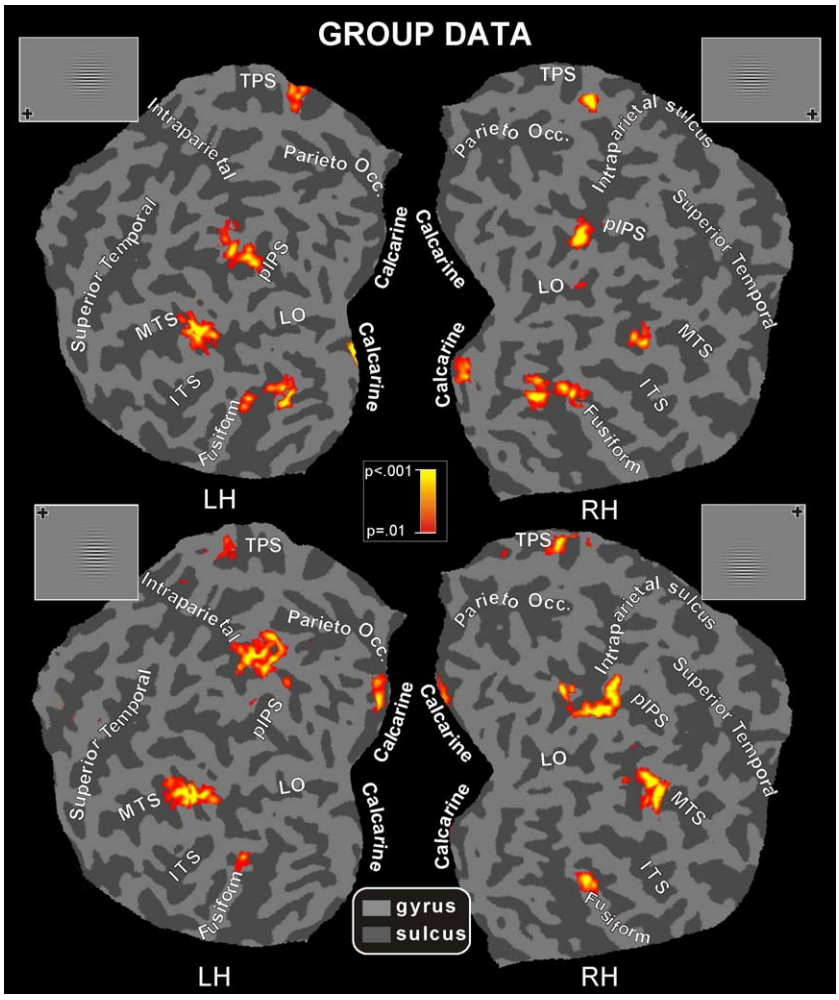

Fig. 4. Group-averaged contralateral fMRI activations for the four quadrants superimposed on the flattened left and right hemispheres of the MNI template. Logo next to each map indicates the visual quadrant stimulated. The pseudocolor scale in the center of the figure indicates the statistical significance of the responses. Major sulci (dark gray) are labeled as follows: parietooccipital sulcus (Parieto Occ.), transverse segment of the parietal sulcus (TPS), intraparietal sulcus (intraparietal), lateral occipital sulcus (LO), superior temporal sulcus (Superior Temporal), middle temporal sulcus (MTS), inferior temporal sulcus (ITS), and calcarine fissure (Calcarine). The fusiform gyrus is labeled "Fusiform".

not likely that P125/N135 is the evoked response to the second (reset) pattern reversal of each stimulus, because the 50-ms delay between the P125/N135 and N75/P85 peaks is shorter than the 66-ms interval between the first and second pattern reversals. Furthermore, it is unlikely that the second pattern reversal would invert the sign of the source dipole if it were in fact generated by a similar volley of synapses on the same part of the dendritic tree as the volley that generated the initial N75/P85. The P125/N135 component may not be apparent in the pattern-onset VEP because of its low amplitude in relation to the overlapping posterior N1 component. In line with this hypothesis, the posterior N1 component of the pattern-onset VEP for upper field stimuli was found to be smaller than for lower field stimuli (e.g., see Fig. 4 of Di Russo et al., 2001), which could result from algebraic summation with a positive component like the upper-field P125 observed in the present experiment.

The P95 component overlapped spatially and temporally with the N75/P85 but was distributed more laterally and was less sensitive to stimulus position. This component could be modeled by a dipolar source in the occipitotemporal cortex near the site of fMRI activation in area MT/V5. The short onset latency of this component is compatible with the view that MT/V5 receives a direct projection from V1 (McKeefry et al., 1997; Probst et al., 1993; Tzelepi et al., 2001; Vanni et al., 2004; Van Rullen and Thorpe, 2001). The motion-sensitive area V5 is probably activated by pattern-reversal stimuli because such reversal produces a clear perception of movement and can be described in terms of motion onset and offset responses (Kubova et al., 1995; Spekreijse et al., 1985). Activation of MT/V5 was not found for pattern-onset stimuli that were not associated with a perception of motion (Di Russo et al., 2001). The P95 component does not correspond to the classical pattern-reversal P100 (Halliday, 1993), which differs in scalp topography and timing. The P100 component reported in previous studies had a peak latency ranging between 100 and 140 ms (e.g., Tumas and Sakamoto, 1997) and was attributed to generators in the calcarine cortex (e.g., Nakamura et al., 2000), suggesting that it corresponds instead to the component labeled P125/N135 in the present study. Finally, the P95 component did not resemble the P100 evoked by pattern-onset stimuli, which had a longer peak latency and was localized to sources in more dorsomedial regions of the occipital cortex (Di Russo et al., 2001).

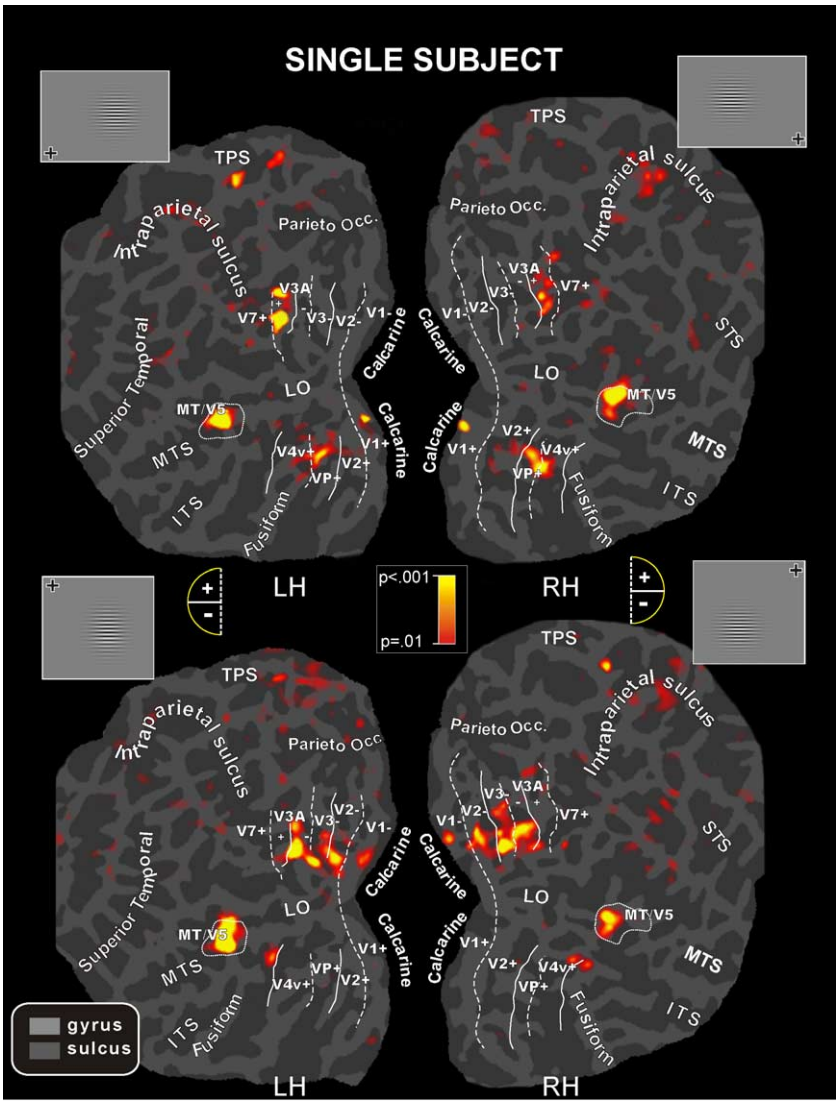

Fig. 5. Flattened left and right hemispheres of an individual participant. The flattened surfaces indicate the contralateral activations found in response to pattern-reversal stimulation of the four quadrants of the visual field in relation to the boundaries of other visual areas defined in the same subjects by the visual field sign (Sereno et al., 1995) and the MT/V5 mapping (Tootell and Taylor, 1995). As indicated in the semicircular logo, dashed and solid lines correspond to vertical and horizontal meridians, respectively; plus and minus symbols refer to upper and lower visual field representations, respectively. The pseudocolor scale in the center of the figure indicates the statistical significance of the responses. Other labels and logos are as in Fig. 4.

The N150 component observed in the present study is very similar in timing and topography to the anterior N1 (N155) evoked by pattern-onset stimuli (Di Russo et al., 2001, 2003). Both the N150 and N155 were localized to generators in and around the TPS. This N150 is clearly different from the N145 typically reported in pattern-reversal studies (see Introduction), which had a medial posterior distribution and was localized to a calcarine source (e.g., Hatanaka et al., 1997). Most likely, the previously reported pattern-shift N145 corresponds to the N135 observed in the present study, which was also localized to calcarine cortex.

Components following N145 have not been emphasized in previous studies of the pattern-reversal VEP. In the present experiment, a posterior, bilateral N160 was observed, which was localized to ventral occipital generators (areas VP, V4v, and V4/V8). The retinotopic organization of these areas resulted in areas VP and V4v being activated by upper field stimuli and area V4/V8 by both upper and lower stimuli (see Fig. 4), in agreement with previous reports (Hadjikhani et al., 1998; Tootell and Hadjikhani, 2001; Wandell, 1999). Similar ventral occipital sources were found to contribute to late negative components (N170–180) in pattern-onset studies (Di Russo et al., 2001, 2003). The pattern-reversal component of longest latency analyzed here was the N180, which was localized to sources in the vicinity of area V3A. Di Russo et al. (2001) found that dipolar sources near V3A could account for a biphasic P110/N170 complex in response to pattern-onset stimuli; similarly, the V3A source in the present study showed a biphasic P120/N180 waveform. These late negative components showed 5- to 15-ms delays in peak activity for ipsilateral vs. contralateral sources, in line with the delays observed in pattern-onset studies (e.g., Clark et al., 1995; Di Russo et al., 2003).

It should be cautioned that the use of hemodynamic imaging to substantiate the estimated locations of ERP sources, as was

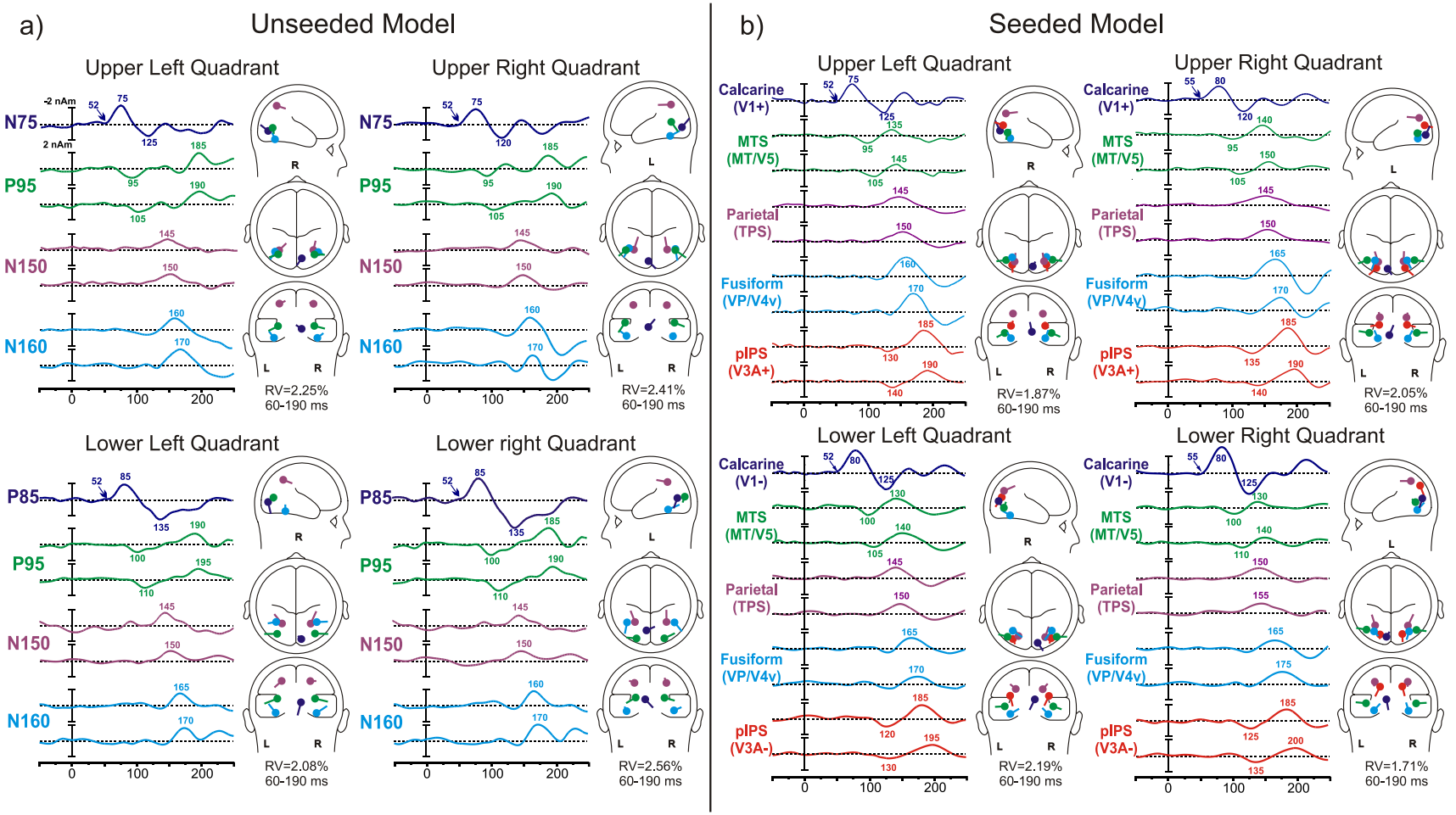

Fig. 6. (a) Unseeded dipole models for each quadrant. The first dipole of each pair is in the contralateral hemisphere. The waveforms in the left side indicate the time course of each dipole (source waveform). Dipoles are labeled according to the component to which they were fit. (b) Dipole models for each quadrant seeded to the fMRI activations. The first dipole of each pair is in the contralateral hemisphere. The waveforms in the left side indicate the time course of each dipole (source waveform). Dipoles are labeled according the seeded fMRI areas.

Table 4
Talairach coordinates of the dipole in the unseeded source model (values are in mm)

Upper left	x	y	z	Upper right	x	y	z
Calcarine (N75)	10	−78	0	Calcarine (N75)	−3	−84	1
Dorsal occipital (P95)	±32	−71	7	Dorsal occipital (P95)	±45	−62	12
Ventral occipital (160)	±39	−65	−15	Ventral occipital (160)	±43	−59	−14
Parietal (N150)	±30	−62	49	Parietal (N150)	±31	−61	46
Lower left	**x**	**y**	**z**	**Lower right**	**x**	**y**	**z**
Calcarine (P85)	9	−87	4	Calcarine (P85)	−8	−73	10
Dorsal occipital (P95)	±35	−77	11	Dorsal occipital (P95)	±25	−87	13
Ventral occipital (160)	±37	−51	−16	Ventral occipital (160)	±42	−53	−10
Parietal (N150)	±26	−56	46	Parietal (N150)	±28	−53	42

done in the present and previous studies (Bonmassar et al., 2001; Di Russo et al., 2001, 2003; Heinze et al., 1994; Mangun et al., 2001; Martinez et al., 1999, 2001; Snyder et al., 1995; Vanni et al., 2004), is subject to certain caveats. First and foremost is the assumption that the hemodynamic response obtained with fMRI or PET is driven by the same neural activity that gives rise to ERP. With regard to visual-evoked activity, such a correspondence appears to be optimal for human medial occipital cortex (including the calcarine fissure) and is less definite for extrastriate visual areas (Gratton et al., 2001). Moreover, it stands to reason that a more accurate dipole model can be achieved for the initial VEP component than for subsequent components, which receive contributions from multiple, spatially and temporally overlapping cortical generators.

Despite these caveats, several considerations lend support to the validity of the present dipole modeling approach. First, and most important, small retinotopically localized stimuli are known to activate rather small regions of early visual areas, often extending across only a small portion of a gyrus or sulcus (Tootell et al., 1998). This makes it reasonable to model the source for a single visual area (or for two retinotopically aligned visual areas) as a single dipole. Second, the representations of a particular location in the visual field in several adjoining visual areas are often close to each other (e.g., upper visual field points in V4v and VP or lower visual field points in V2 and V3). While this makes it difficult to distinguish the individual contributions of adjoining areas, it also makes it appropriate to collapse their combined activity into a single source. Third, the number of dipoles chosen to fit the VEP was strictly determined by the number of topographically distinctive components in the waveform rather than by an arbitrary criterion of goodness of fit. Finally, the close correspondence between the unconstrained dipole model and the model seeded to the active fMRI foci lends support to the general accuracy of the source localizations proposed for these VEP components.

In summary, the present study combined VEP recording with structural and functional MRI and retinotopic mapping of visual cortical areas to support the hypothesis that the initial evoked components to pattern-shift stimuli (N75/P85 and P125/N135) arise from neural generators in the primary visual cortex while subsequent components (P95, N150, N160, and N180) are generated in multiple extrastriate occipital and parietal cortical areas. This analysis should enhance the information value of the pattern-shift VEP both as an index of neurological dysfunction of the visual pathways (Halliday, 1993) and as a tool for studying the cortical mechanisms of visual-perceptual processing.

Acknowledgments

This research was supported by Italian grants from MIUR and IUSM to DS and FDR, and by NIMH (USA) grant MH-25594 to SAH.

References

Aine, C.J., Supek, S., George, J.S., Ranken, D., Lewine, J., Sanders, J., Best, E., Tiee, W., Flynn, E.R., Wood, C.C., 1996. Retinotopic organization of human visual cortex: departures from the classical model. Cereb. Cortex 6, 354–361.

Barrett, G., Blumhardt, L., Halliday, A.M., Halliday, E., Kriss, A., 1976. A paradox in the lateralization of the visual evoked response. Nature 261, 253–255.

Biersdorf, W.R., 1987. Different scalp localization of pattern onset and reversal visual evoked potentials. Doc. Ophthalmol. 66, 313–320.

Bonmassar, G., Schwartz, D.P., Liu, A.K., Kwong, K.K., Dale, A.M., Belliveau, J.W., 2001. Spatiotemporal brain imaging of visual-evoked activity using interleaved EEG and fMRI recordings. NeuroImage 13, 1035–1043.

Brecelj, J., Kakigi, R., Koyama, S., Hoshiyama, M., 1998. Visual evoked magnetic responses to central and peripheral stimulation: simultaneous VEP recordings. Brain Topogr. 10, 227–237.

Clark, V.P., Fan, S., Hillyard, S.A., 1995. Identification of early visually evoked potential generators by retinotopic and topographic analysis. Hum. Brain Mapp. 2, 170–187.

Dale, A.M., Fischl, B., Sereno, M.I., 1999. Cortical surface-based analysis: I. segmentation and surface reconstruction. NeuroImage 9, 179–194.

Di Russo, F., Martínez, A., Sereno, M.I., Pitzalis, S., Hillyard, S.A., 2001. The cortical sources of the early components of the visual evoked potential. Hum. Brain Mapp. 15, 95–111.

Di Russo, F., Martínez, A., Hillyard, S.A., 2003. Source analysis of event-related cortical activity during visuo-spatial attention. Cereb. Cortex 13, 486–499.

Ducati, A., Fava, E., Motti, E.D., 1988. Neuronal generators of the visual evoked potentials: intracerebral recording in awake humans. Electroencephalogr. Clin. Neurophysiol. 71, 89–99.

Dumoulin, S.O., Hoge, R.D., Baker Jr., C.L., Hess, R.F., Achtman, R.L., Evans, A.C., 2003. Automatic volumetric segmentation of human visual retinotopic cortex. NeuroImage 18, 576–587.

Felleman, D.J., Van Essen, D.C., 1991. Distributed hierarchical processing in the primate cerebral cortex. Cereb. Cortex 1, 1–47.

Fischl, B., Sereno, M.I., Dale, A.M., 1999. Cortical surface-based analysis. II: inflation, flattening, and a surface-based coordinate system. NeuroImage 9, 195–207.

Gratton, G., Goodman-Wood, M.R., Fabiani, M., 2001. Comparison of neuronal and hemodynamic measures of the brain response to visual stimulation: an optical imaging study. Hum. Brain Mapp. 13, 13–25.

Hadjikhani, N., Liu, A.K., Dale, A.M., Patrick Cavanagh, P., Tootell, R., 1998. Retinotopy and colour sensitivity in human visual cortical area V8. Nat. Neurosci. 1, 235–241.

Haimovic, I.C., Pedley, T.A., 1982. Hemi-field pattern reversal visual evoked potentials: I. Normal subjects. Electroencephalogr. Clin. Neurophysiol. 54, 111–120.

Halliday, A.M., 1993. Evoked Potentials in Clinical Testing. Churchill Livingstone, Edinburgh.

Hashimoto, T., Kashii, S., Kikuchi, M., Honda, Y., Nagamine, T., Shibasaki, H., 1999. Temporal profile of visual evoked responses to pattern reversal stimulation analyzed with a whole-head magnetometer. Exp. Brain Res. 125, 375–382.

Hatanaka, K., Nakasato, N., Seki, K., Kanno, A., Mizoi, K., Yoshimoto, T., 1997. Striate cortical generators of the N75, P100 and N145 components localized by pattern-reversal visual evoked magnetic fields. Tohoku J. Exp. Med. 182, 9–14.

Heinze, H.J., Mangun, G.R., Burchert, W., Hinrichs, H., Scholz, M., Munte, T.F., Gos, A., Johannes, S., Scherg, M., Hundeshagen, H., Gazzaniga, M.S., Hillyard, S.A., 1994. Combined spatial and temporal imaging of spatial selective attention in humans. Nature 392, 543–546.

Hoeppner, T.J., Bergen, D., Morrell, F., 1984. Hemispheric asymmetry of visual evoked potentials in patients with well-defined occipital lesions. Electroencephalogr. Clin. Neurophysiol. 57, 310–319.

Kubova, Z., Kuba, M., Spekreijse, H., Blakemore, C., 1995. Contrast dependence of motion-onset and pattern-reversal evoked potentials. Vision Res. 35, 197–205.

Lehmann, D., Darcey, T.M., Skrandies, W., 1982. Intracerebral and scalp fields evoked by hemiretinal checkerboard reversal, and modeling of their dipole generators. Adv. Neurol. 32, 41–48.

Lueck, C.J., Zeki, S., Friston, K.J., Deiber, M.P., Cope, P., Cunningham, V.J., Lammertsma, A.A., Kennard, C., Frackowiak, R.S., 1989. The colour centre in the cerebral cortex of man. Nature 340, 386–389.

Maier, J., Dagnelie, G., Spekreijse, H., Van Dijk, B.W., 1987. Principal component analysis for source localization VEPs in man. Vision Res. 27, 165–177.

Mangun, G.R., Hinrichs, H., Scholz, M., Mueller-Gaertner, H.W., Herzog, H., Krause, B.J., Tellman, L., Kemna, L., Heinze, H.J., 2001. Integrating electrophysiology and neuroimaging of spatial selective attention to simple isolated visual stimuli. Vision Res. 41, 1423–1435.

Martinez, A., Anllo-Vento, L., Sereno, M.I., Frank, L.R., Buxton, R.B., Dubowitz, D.J., Wong, E.C., Hinrichs, H., Heinze, H.J., Hillyard, S.A., 1999. Involvement of striate and extrastriate visual cortical areas in spatial attention. Nat. Neurosci. 2, 364–369.

Martinez, A., Di Russo, F., Anllo-Vento, L., Sereno, M.I., Buxton, R.B., Hillyard, S.A., 2001. Putting spatial attention on the map: timing and localization of stimulus selection processes in striate and extrastriate visual areas. Vision Res. 41, 1437–1457.

McKeefry, D.J., Watson, J.D., Frackowiak, R.S., Fong, K., Zeki, S., 1997. The activity in human areas V1/V2, V3, and V5 during the perception of coherent and incoherent motion. NeuroImage 5, 1–12.

Michael, W.F., Halliday, A.M., 1971. Differences between the occipital distribution of upper and lower field pattern evoked responses in man. Brain Res. 32, 311–324.

Nakamura, A., Kakigi, R., Hoshiyama, M., Koyama, S., Kitamura, Y., Shimojo, M., 1997. Visual evoked cortical magnetic fields to pattern reversal stimulation. Brain. Res. Cogn. Brain Res. 6, 9–22.

Nakamura, M., Kakigi, R., Okusa, T., Hoshiyama, M., Watanabe, K., 2000. Effects of check size on pattern reversal visual evoked magnetic field and potential. Brain Res. 28, 77–86.

Noachtar, S., Hashimoto, T., Luders, H., 1993. Pattern visual evoked potentials recorded from human occipital cortex with chronic subdural electrodes. Electroencephalogr. Clin. Neurophysiol. 88, 435–446.

Onofrj, M., Fulgente, T., Malatesta, G., Ferracci, F., 1993. Visual evoked potentials (VEP) to altitudinal stimuli: effect of stimulus manipulations on VEP scalp topography. Clin. Vis. Sci. 8, 529–544.

Onofrj, M., Fulgente, T., Thomas, A., Malatesta, G., Peresson, M., Locatelli, T., Martinelli, V., Comi, G., 1995a. Source model and scalp topography of pattern reversal visual evoked potentials to altitudinal stimuli suggest that infoldings of calcarine fissure are not part of VEP generators. Brain Topogr. 7, 217–231.

Onofrj, M., Fulgente, T., Thomas, A., Curatola, L., Peresson, M., Lopez, L., Locatelli, T., Martinelli, V., Comi, G., 1995b. Visual evoked potentials generator model derived from different spatial frequency stimuli of visual field regions and magnetic resonance imaging coordinates of V1, V2, V3 areas in man. Int. J. Neurosci. 83, 213–239.

Probst, T., Plendl, H., Paulus, W., Wist, E.R., Scherg, M., 1993. Identification of the visual motion area (area V5) in the human brain by dipole source analysis. Exp. Brain Res. 93, 345–351.

Schiller, P.H., Dolan, R.P., 1994. Visual aftereffects and the consequences of visual system lesions on their perception in the rhesus monkey. Vis. Neurosci. 11, 643–665.

Schroeder, C.E., Steinschneider, M., Javitt, D.C., Tenke, C.E., Givre, S.J., Mehta, A.D., Simpson, G.V., Arezzo, J.C., Vaughan Jr., H.G., 1995. Localization of ERP generators and identification of underlying neural processes. Electroencephalogr. Clin. Neurophysiol., Suppl. 44, 55–75.

Seki, K., Nakasato, N., Fujita, S., Hatanaka, K., Kawamura, T., Kanno, A., Yoshimoto, T., 1996. Neuromagnetic evidence that the P100 component of the pattern reversal visual evoked response originates in the bottom of the calcarine fissure. Electroencephalogr. Clin. Neurophysiol. 100, 436–442.

Sereno, M.I., Dale, A.M., Reppas, J.B., Kwong, K.K., Belliveau, J.W., Brady, T.J., Rosen, B.R., Tootell, R.B., 1995. Borders of multiple visual areas in humans revealed by functional magnetic resonance imaging. Science 268, 889–893.

Shigeto, H., Tobimatsu, S., Yamamoto, T., Kobayashi, T., Kato, M., 1998. Visual evoked cortical magnetic responses to checkerboard pattern reversal stimulation: a study on the neural generators of N75, P100 and N145. J. Neurol. Sci. 156, 186–194.

Slotnick, S.D., Klein, S.A., Carney, T., Sutter, E., Dastmalchi, S., 1999. Using multi-stimulus VEP source localization to obtain a retinotopic map of human primary visual cortex. Clin. Neurophysiol. 110, 793–800.

Snyder, A.Z., Abdullaev, Y.G., Posner, M.I., Raichle, M.E., 1995. Scalp electrical potentials reflect regional cerebral blood flow responses during processing of written words. Proc. Natl. Acad. Sci. U. S. A. 92, 1689–1693.

Spekreijse, H., Dagnelie, G., Maier, J., Regan, D., 1985. Flicker and movement constituents of the pattern reversal response. Vision Res. 25, 1297–1304.

Tabuchi, H., Yokoyama, T., Shimogawara, M., Shiraki, K., Nagasaka, E., Miki, T., 2002. Study of the visual evoked magnetic field with the M-sequence technique. Invest. Ophthalmol. Visual Sci. 43, 2045–2054.

Talairach, J., Tournoux, P., 1988. Co-Planar Stereotaxic Atlas of the Human Brain. Thieme, New York, NY.

Tobimatsu, S., 2002. Transient and steady-state VEPs-reappraisal. Int. Congr. Ser. 1232, 207–211.

Tootell, R.B., Hadjikhani, N.K., 2001. Where is 'dorsal V4'in human visual cortex? Retinotopic, topographic and functional evidence. Cereb. Cortex 11, 298–311.

Tootell, R.B.H., Taylor, J.B., 1995. Anatomical evidence for MT and additional cortical visual areas in humans. Cereb. Cortex 5, 39–55.

Tootell, R.B., Mendola, J.D., Hadjikhani, N.K., Ledden, P.J., Liu, A.K., Reppas, J.B., Sereno, M.I., Dale, A.M., 1997. Functional analysis of V3A and related areas in human visual cortex. J. Neurosci. 15, 7060–7078.

Tootell, R.B., Mendola, J.D., Hadjikhani, N.K., Liu, A.K., Dale, A.M., 1998. The representation of the ipsilateral visual field in human cerebral cortex. Proc. Natl. Acad. Sci. U. S. A. 95, 818–824.

Tumas, V., Sakamoto, C., 1997. Comparison of the mechanisms of latency shift in pattern reversal visual evoked potential induced by blurring and contrast reduction. Electroencephalogr. Clin. Neurophysiol. 104, 96–100.

Tzelepi, A., Ioannides, A.A., Poghosyan, V., 2001. Early (N70m) neuromagnetic signal topography and striate and extrastriate generators following pattern onset quadrant stimulation. NeuroImage 13, 702–718.

Van Rullen, R., Thorpe, S.J., 2001. The time course of visual processing: from early perception to decision-making. J. Cogn. Neurosci. 13, 454–461.

Vanni, S., Tanskanen, T., Seppa, M., Uutela, K., Hari, R., 2001. Coinciding early activation of the human primary visual cortex and anteromedial cuneus. Proc. Natl. Acad. Sci. U. S. A. 98, 2776–2780.

Vanni, S., Warnking, J., Dojat, M., Delon-Martin, C., Bullier, J., Segebarth, C., 2004. Sequence of pattern onset responses in the human visual areas: an fMRI constrained VEP source analysis. NeuroImage 21, 801–817.

Wandell, B.A., 1999. Computational neuroimaging of human visual cortex. Annu. Rev. Neurosci. 22, 145–147.

Zeki, S., Bartels, A., 1999. The clinical and functional measurement of cortical (in) activity in the visual brain, with special reference to the two subdivisions (V4 and V4 alpha) of the human colour centre. Philos. Trans. R. Soc. Lond., B Biol. Sci. 354, 1371–1382.